ACS OMEGA

Open Access

http://pubs.acs.org/journal/acsodf

Article

HNTs Improve Flame Retardant and Thermal Insulation of the PVA/CA Composite Aerogel

Taopeng Yang, Jiayou Xu,* and Shu Lv

Cite This: *ACS Omega* 2024, 9, 40608−40617

Read Online

ACCESS | Metrics & More | Article Recommendations | Supporting Information

ABSTRACT: Porous materials are widely used in construction, batteries, electrical appliances, and other fields. In order to meet the demand for flame-retardant and thermal insulation properties of organic porous materials, in this work, poly(vinyl alcohol)/calcium alginate/halloysite nanotube (PVA/CA/HNTs) aerogels with a hierarchical pore structure at micrometer−nanometer scales were prepared through freeze-drying using PVA as the substrate. The cross-linking reactions of PVA with H_3BO_3 and sodium alginate (SA) with $CaCl_2$ constructed a double cross-linking network structure within the aerogel. And the HNTs were incorporated as reinforcing agents. The experimental results showed that the PVA/CA/HNTs aerogels had excellent flame-retardant and thermal insulation properties, and the heat release rate (HRR) and total heat release (THR) were effectively reduced compared to the PVA/CA aerogel. In addition, PVA/CA/HNTs aerogels had a high limiting oxygen index (LOI 60%) and low thermal conductivity (0.040 W/m·K). While their surface was subjected to a flame (800−1000 °C) for 25 min, the temperatures of the back surface were still lower than 80 °C. The low thermal conductivity of HNTs with hollow nanotube-like structures and the excellent flame-retardant properties of CA contributed to this phenomenon. The presence of HNTs and CA facilitated the formation of a dense carbon layer during combustion, enhancing the flame retardancy for PVA. In addition, the interpenetrating cross-linking network and the unique nanopores of HNTs collectively established a hierarchical pore structure within the gel, effectively impeding substance and heat exchange between the substrate and external environment. As the flame-retardant and thermal insulating material, PVA/CA/HNTs aerogels have a promising development prospect and potential in the fields of construction, transportation, electronics, and electrical appliances.

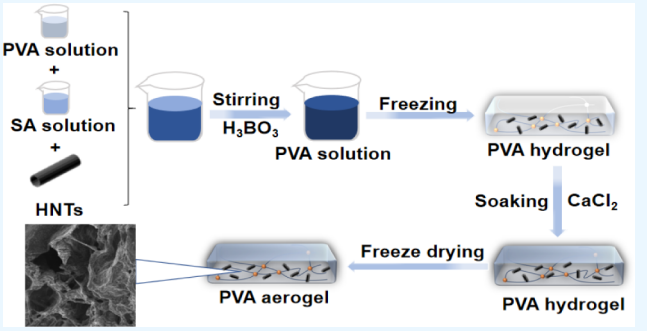

1. INTRODUCTION

Aerogel generally refers to a three-dimensional porous network-like gel formed by replacing the liquid phase in hydrogel with gas through supercritical drying or freeze-drying.[1,2] As a new type of functional polymer materials, polymer aerogels have the advantages of low thermal conductivity, low density, high specific area, high porosity, etc,[3−5] so that they can be used in many fields, such as sound-absorbing materials,[6,7] oil−water separation materials,[8,9] electromagnetic shielding materials,[10,11] flame-retardant and thermal insulation materials.[12,13] Up to now, a variety of biodegradable polymers have been used for the construction of composite aerogels, including polyvinyl alcohol,[14] polylactic acid,[15] chitosan,[16] nanocellulose,[17] alginate,[18] phytic acid,[19] and so on. Polymer aerogels are less dense, more flexible, and more biocompatible than conventional inorganic aerogels.[20−22] However, the addition of flammable polymers may make the aerogel's fire-retardant and thermal insulation performance decrease, which creates certain safety hazards.[23] Therefore, the development of composite aerogels with high fire resistance and strong mechanical properties is a top priority.

Polyvinyl alcohol is an environmental, renewable, and degradable polymer material with good film-forming, bonding, and thermal stability,[24−26] which makes it an ideal matrix material for the preparation of flame-retardant and heat-insulating aerogels. However, the LOI of PVA is only about 20.6%,[27] indicating its high flammability. It would lead to the generation of large amounts of heat, soot, and toxic gases during combustion, which greatly limits its applications. In order to solve these problems, phosphorus-containing flame retardants,[28] nitrogen-containing flame retardants,[29] and intumescent flame retardants (IFRs)[30,31] are added to improve the flame-retardant properties, of which IFR consists of an acid source, a carbon source, and a gas source and forms an intumescent char layer during combustion to provide flame

Received: May 6, 2024
Revised: August 16, 2024
Accepted: August 27, 2024
Published: September 19, 2024

retardancy. However, the traditional flame retardants come from petrochemical resources, which are nonrenewable resources, so people are beginning to turn to renewable resources and biomass resources. Tan[32] modified PVA by utilizing the multiple cross-linking structure of hexachlorocyclotriphosphazene derivatives (SHCP) and chitosan (CS) followed by Cu^{2+} chelation, to produce flame-retardant, smoke-suppressing, and antimicrobial PVA composites. Not only were the HRR and THR of the composites greatly reduced but also the char-forming ability of the materials was greatly improved.

SA is a natural polysaccharide whose molecule consists of a linear copolymer of β-D-mannuronic acid (M-unit) and α-L-guluronic acid (G-unit) linked by a (1→4) bond.[33] It can react with Ca^{2+} to form eggshell-shaped CA, which is used in flame-retardant and thermal insulation applications.[34] The presence of metal ions causes the aerogel to create an alkaline environment during combustion, causing the alginate fibers to undergo a decarboxylation reaction to produce CO_2 and reduce the O_2 concentration in the surrounding environment. Alginate macromolecular chains can also form cross-linking structures by chelating with metal ions, changing the structure of the material to increase its pyrolysis temperature. At the same time, the addition of metal ions also enables the aerogel to produce metal oxides or metal carbonates that cover its surface during combustion, insulating it from air and flame.[35]

To improve the mechanical properties and flame-retardant properties of PVA, inorganic nanofillers such as magnesium hydroxide,[36] carbon nanoparticles,[37] and graphene[38] can be added optionally. HNTs are natural nanomaterials with a hollow tubular structure. Lv[39] prepared HNTs/PVA composite aerogels with high thermal insulation performance by adjusting the solid concentration. The unique hollow tube structure of HNTs gives aerogels excellent spatial structure, flame-retardant, and thermal insulation properties. Hence, the PVA/CA/HNTs composite aerogels were designed and synthesized using a facile freeze-drying method, which allowed efficient preparation of hierarchical pore structure of aerogels. The cross-linking reactions of PVA with H_3BO_3 and SA with $CaCl_2$ constructed a double cross-linking network structure within the PVA/CA aerogel. Then, the PVA/CA/HNTs aerogel was prepared by incorporating HNTs. H_3BO_3, CA, and PVA are excellent flame-retardant materials, which can be dispersed evenly in PVA solution. The size of the pores of the double cross-linked network formed by PVA and CA is mainly in the micrometer scale, and the incorporation of HNTs endowed the aerogel with more nanoscale pores. In this way, the aerogel's fire-retardant insulation properties and structural stability are ensured. Its flame-retardant and heat insulation mechanisms are embodied in the following two aspects. On the one hand, a decarboxylation reaction occurred during CA combustion to generate CO_2, which diluted O_2 and gaseous combustibles inside the aerogel. During combustion, metal oxides and metal carbonates covering the aerogel surface were generated, which played a role in isolating the flame from the air. On the other hand, CA and PVA formed a double cross-linked interpenetrating network structure inside the aerogel, along with a great char formation ability. On this basis, the high specific area and nanotubular structure of HNTs could help the aerogel form a hierarchical pore structure. It not only effectively reduced the thermal conductivity of the aerogel, improving the thermal insulation performance, but also played the role of skeleton support inside the aerogel, which synergized with PVA/CA/H_3BO_3 to promote the formation of hybrid char barrier, effectively enhancing the flame-retardant performance. In this work, the effects of different additions of HNTs on the morphology and mechanical properties of the PVA/CA/HNTs aerogels were compared. Moreover, the flame retardancy, smoke suppression properties, and thermal insulation of the composites of PVA/CA/HNTs aerogels were systematically investigated.

2. EXPERIMENTAL

2.1. Materials. Polyvinyl alcohol (PVA, 97%) was purchased from Zhiyuan Chemical Reagent Corporation (Tianjin, China). Calcium chloride ($CaCl_2$, 96%) was purchased from Zhiyuan Chemical Reagent Corporation (Tianjin, China). Boric acid (H_3BO_3, 99.5%) was purchased from Xilong Science Co. Ltd. (Shantou, China). Sodium alginate (SA) was purchased from Xilong Science (Shantou, China). HNTs were purchased from Lingshou County Tuyun Mineral Product Processing Co. Ltd. (Shijiazhuang, China). All chemicals were of laboratory grade and were used directly without further purification.

2.2. Preparation of the PVA/CA/HNTs Aerogels. The preparation process of the PVA/CA/HNTs aerogels is schematically exhibited in Figure 1. First, 8 wt % of PVA

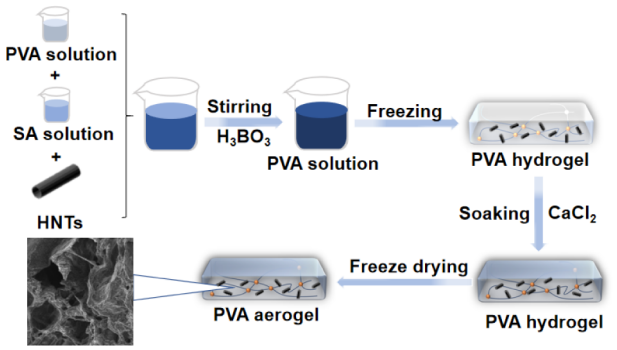

Figure 1. Schematic for the PVA aerogel preparation process.

aqueous solution was prepared by dissolving 8 g PVA in 92 mL DI water under stirring at 90 °C for 2 h. 2 wt % of SA solution was prepared by dissolving 2 g SA powder in 98 g DI water. After that, 100 g PVA solution and 40 g SA solution were fully mixed and stirred in beakers. Simultaneously, 0, 2, 6, and 10 g of HNTs were added separately to obtain PVA/CA/HNTs solution. Furthermore, 10 g 6 wt % of H_3BO_3 was added drop by drop to the above solution. After stirring thoroughly, the solution was poured into the mold and frozen in the refrigerator for 10 h to form hydrogel. Finally, the frozen hydrogel was soaked in 5 wt % $CaCl_2$ solution for 24 h and then frozen-dried under vacuum conditions of −50 °C to obtain the PVA/CA/HNTs aerogels. The aerogels prepared above were denoted as PVA/CA/HNTs-0, PVA/CA/HNTs-2, PVA/CA/HNTs-6, and PVA/CA/HNTs-10. The formulation of the PVA aerogels is shown in Table 1.

2.3. Characterization. The microstructure of the aerogels was analyzed by a TENSOR II+Hyperion2000 type Fourier transform infrared (FT-IR) spectrometer (Bruker, Germany), using a KBr disk in the measurement range of 4000−500 cm^{-1}. Thermogravimetric analysis (TGA) was performed on a TG-209 F1 instrument (Netzsch, Germany). The tests were carried out in a nitrogen atmosphere with a temperature range of 50−

https://doi.org/10.1021/acsomega.4c04296
ACS Omega 2024, 9, 40608−40617

Table 1. Fabrication of the PVA Aerogels

Sample	PVA (8 wt %)/g	SA (2 wt %)/g	H_3BO_3 (6 wt %)/g	$CaCl_2$ (5 wt %)/g	HNTs/g
PVA/CA/HNTs-0	100	40	10	50	0
PVA/CA/HNTs-2	100	40	10	50	2
PVA/CA/HNTs-6	100	40	10	50	6
PVA/CA/HNTs-10	100	40	10	50	10

700 °C and a heating rate of 10 °C/min. The morphology of the samples was observed by a JSM-7001F scanning electron microscope (SEM) (JEOL, Japan) and a JEM-2100F transmission electron microscope (TEM) (JEOL, Japan). The micropore and mesopore of aerogels were measured by an ASAP2460 fully automatic specific surface area and porosity analyzer (Micromeritics, USA), and all samples were measured after vacuum degassing at 60 °C for 4h. The thermal conductivity of composite aerogels was measured by laser flash at 20 °C using an LFA 447 Laser Flash Apparatus (Netzsch, Germany). The mechanical properties including tensile properties and compressive strength were measured using a UT4304 universal mechanical testing machine (Suns, China). Each sample (50 × 10 × 5 mm^3) was tested at a crosshead speed of 20 mm/min at room temperature. Compression strength was conducted by using the machine, equipped with a 10 kN load cell, at a crosshead of 20 mm/min. Three measurements were made, and average values were calculated. The limited oxygen index (LOI) values of the aerogel samples (120 × 5 × 5 mm^3) were measured according to ASTM D2863-2009 by an HC-2C type oxygen index meter (Jiangning Analysis Instrument Co., Nanjing, China). The UL-94 test was performed on a CZF-2 vertical burning test instrument (Jiangning Analysis Instrument, China) using aerogel sheets (125 × 10 × 5 mm^3). The cone calorimeter test of the aerogel samples (100 × 10 × 10 mm^3) was conducted by a cone calorimeter (Suzhou Vouch Testing Technology, China) at a heat flux of 50 kW/m^2. Flame spray experiments were performed using a butane flame with a center flame temperature of 800−1000 °C. The sample size was 100 × 100 × 5 mm^3. The distance between the flame tip and sample was fixed at 60 mm and perpendicular to the surface of the aerogel. The temperature at the back of the aerogel was measured with an infrared thermometer at 5 min intervals. The rheological properties were characterized using a Caber1 tensile rheometer (ThermoScientific, USA). Dynamic frequency scanning tests were performed over a range of 0.01−100 rad s^{-1} at a temperature of 110 °C.

3. RESULTS AND DISCUSSION

3.1. PVA/SA/HNTs Hydrogel. Using FT-IR spectroscopy, the theoretical basis for the existence of three-dimensional network structures for double cross-linking between PVA/H_3BO_3 and SA/$CaCl_2$ was obtained. The FT-IR spectra of PVA (Figure 2a) showed strong characteristic peaks at 844, 1086, 1412, 2908, and 3268 cm^{-1}, and these peaks, respectively, corresponded to the C−C stretching vibration, C−O crystal-type and amorphous-type stretching vibration, $-CH_2$ asymmetric and symmetric stretching vibration, and O−H stretching vibration.[40−42] The peaks presented in the FT-IR spectra of PVA and PVA/H_3BO_3 (Figure 2a) showed a significant decrease in intensity after the addition of cross-linker H_3BO_3, which was because −OH on PVA and H_3BO_3 formed a stable aldehyde condensate. The weak peak at 600 cm^{-1} was due to the O−B−O bond formed by the addition of a small amount of boric acid.[43]

In the infrared spectrum of SA and CA (Figure 2b), the peak of SA at 2923 cm^{-1} was formed due to the C−H stretching vibration on the six-membered ring of its macromolecule, whereas the peak of CA failed to be formed here. Because the SA macromolecule reacted with Ca^{2+} sufficiently to form a complex structure, it caused the C−H stretching vibration on the six-membered ring to become extremely weak and the peak of absorption to disappear gradually. Similarly, the absorption peak of SA at 3434 cm^{-1} due to the O−H stretching vibration was weakened after the reaction, and the position of the peak was shifted to a lower wavenumber.[44] After the introduction of Ca^{2+}, the intensity of the C−O peak at 1058 cm^{-1} of alginate was significantly reduced,[45] which was because the electrostatic interaction between Ca^{2+} and COO^- effectively inhibited the movement of the molecular chain. PVA was cross-linked with H_3BO_3; besides, $CaCl_2$ reacted with the carboxylate in SA to form CA as a cross-linking agent. They formed PVA hydrogels with an interpenetrating network structure each other. The schematic diagram of the reaction mechanism is shown in Figure 3.

In order to demonstrate the existence of a double cross-linking structure within the PVA aerogel, different components of PVA hydrogels were prepared and tested for viscosity (Figure 2c). Compared with PVA/SA/HNTs, the viscosity of the PVA/H_3BO_3/SA/HNTs increased due to the reaction of −OH on PVA with −OH on H_3BO_3 to form a stable aldehyde condensate. Then, $CaCl_2$ was added to the hydrogel, and the viscosity of the PVA/H_3BO_3/CA/HNTs was further increased

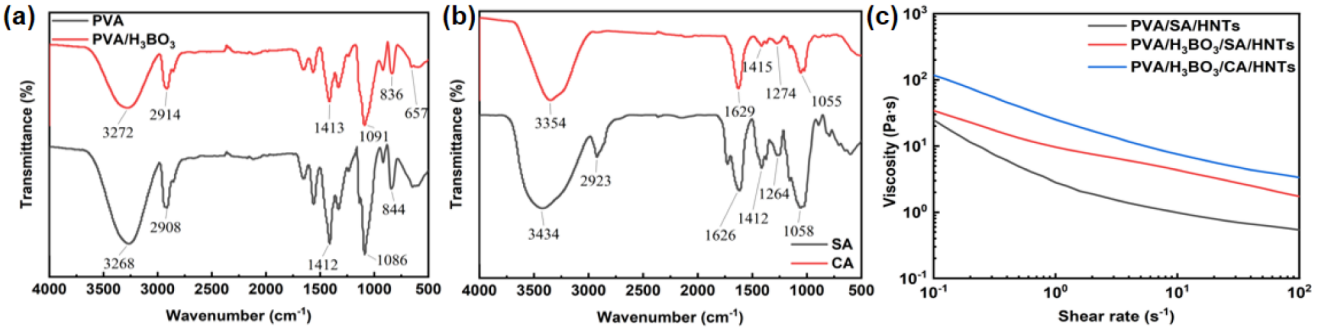

Figure 2. (a) FT-IR spectra of PVA, PVA/H_3BO_3. (b) FT-IR spectra of SA, CA. (c) Viscosity curve of PVA hydrogel with different components.

https://doi.org/10.1021/acsomega.4c04296
ACS Omega 2024, 9, 40608−40617

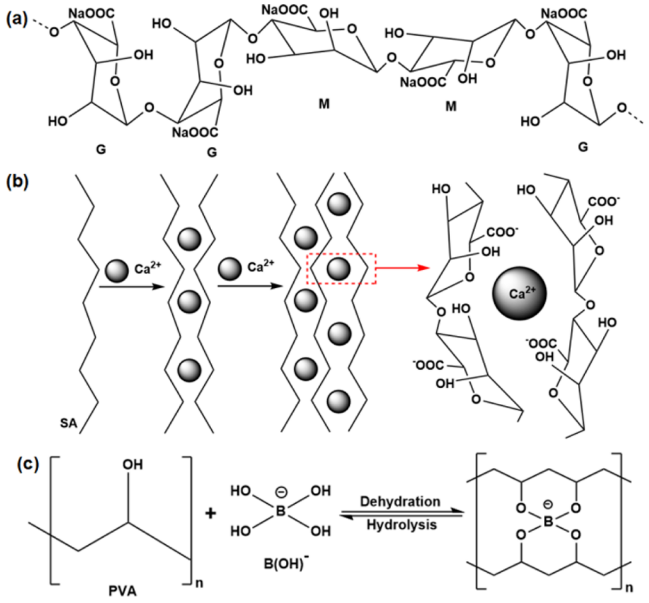

Figure 3. (a) Structure diagram of sodium alginate. (b) Schematic diagram of the reaction mechanism between SA and $CaCl_2$. (c) Schematic diagram of the reaction mechanism between PVA and H_3BO_3.

due to the formation of CA from SA and $CaCl_2$. The formation of an interpenetrating network structure between PVA/H_3BO_3 and CA led to an increase in the intermolecular forces and a decrease in the mobility of the molecular chains.

3.2. Porous Structure of the PVA/CA/HNTs Aerogels. A simple freeze-drying method was used to prepare a series of aerogels using PVA as the matrix and HNTs as the reinforcing agent. In PVA aerogels, a porous network structure existed, and HNTs played the role of a skeleton in the aerogels. The morphology of the cross sections of different PVA aerogels was measured by scanning electron microscopy, as shown in Figures 4a−d. The PVA aerogels all showed a disordered three-dimensional porous network structure, which was mainly attributed to the cross-linking of the −OH group of PVA with H_3BO_3 through dehydration condensation and the −COO− group of SA with Ca^{2+} through an ionic reaction. The polymers formed by these two reactions could be further cross-linked to form interpenetrating network structures. Combined with the transmission electron microscopy images (Figure 4e,f), it could be seen that the HNTs with hollow nanotube-like structures (tube diameters about 15−100 nm) could be better embedded within the aerogel, and a micrometer−nanometer hierarchical pore structure inside the aerogel was thus formed.

In order to further understand the pore structure of the aerogels, its macroporous and nanoporous structures were analyzed, respectively. The pore size distribution of the macropores of the PVA aerogels is shown in Figure S1a−d, where different HNTs contents led to the formation of different pore sizes, and the pore size distributions were mainly concentrated in the range of tens of micrometers. Notably, the average diameter of the PVA aerogels micropores decreased from 66.2 to 39.6 μm with the increase of HNTs content, and the overall distribution was more uniform. This was due to the fact that the pores formed by double cross-linking were filled with more HNTs, which in turn could give the aerogels better thermal insulation properties.

Figure S1e shows the N_2 adsorption−desorption isotherms of the PVA aerogels with different HNTs contents. It was worth nothing that PVA/CA/HNTs-0 did not show adsorption−desorption isotherms and nanoporous distribution. The addition of HNTs effectively prevented the collapse of the pore structure due to its skeleton role inside the PVA aerogels, so the PVA/CA/HNTs aerogels showed the isotherms and porous distribution. Their isotherms belonged to type IV isotherms, which meant that PVA/CA/HNTs aerogels exhibited good nanoporous structures. The distribution of nanoporous pore diameters of the PVA aerogel was determined by the Barrett−Joyner−Halenda (BJH) method. It could be clearly seen from Figure S1f that the average diameter of nanopores of the PVA/CA/HNTs aerogel increased with the addition of HNTs, and the PVA/CA/HNTs-10 aerogel was the largest. The PVA/CA/HNTs aerogels' pore size was smaller than the free diameter of air (about 70 nm), which made the air molecules existing inside the pores lose the ability of free circulation. It greatly reduced the efficiency of heat transfer and played an effective role in flame-retardant insulation.

3.3. Properties of the PVA/CA/HNTs Aerogels. The basic properties of different PVA aerogels are shown in Table 2. With the increase in content of HNTs, the porosity of PVA

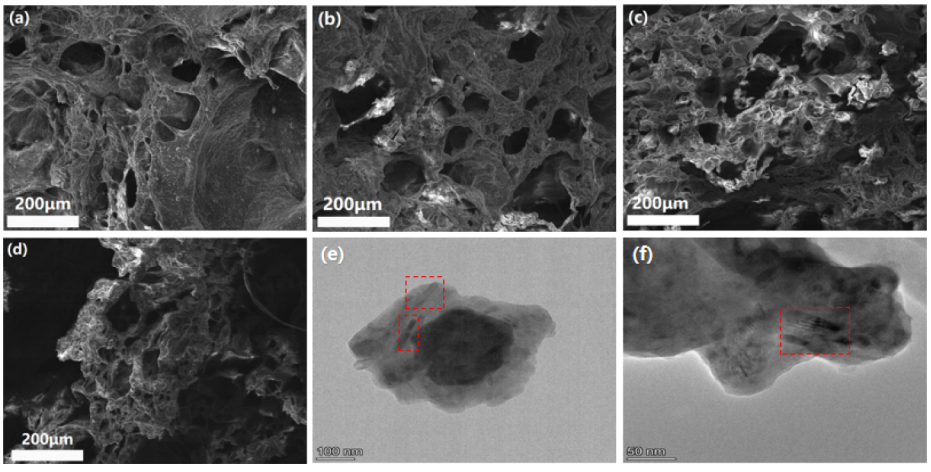

Figure 4. SEM images of the PVA aerogels with different addition of HNTs. (a) PVA/CA/HNTs-0. (b) PVA/CA/HNTs-2. (c) PVA/CA/HNTs-6. (d) PVA/CA/HNTs-10. TEM images of the HNTs and aerogel. (e) HNTs and (f) PVA aerogel.

https://doi.org/10.1021/acsomega.4c04296
ACS Omega 2024, 9, 40608−40617

Table 2. Properties of the PVA Aerogels

Sample	Density (g/cm^3)	Porosity (%)	Compressive modulus (MPa)	Thermal conductivity (W/m·k)
PVA/CA/HNTs-0	0.895	59.32	2.199	0.057
PVA/CA/HNTs-2	0.915	58.41	2.234	0.047
PVA/CA/HNTs-6	1.055	52.05	2.389	0.046
PVA/CA/HNTs-10	1.105	49.75	2.456	0.040

aerogel decreased from 59.32% to 49.75%, respectively, and the density increased from 0.895 to 1.105 g/cm^3, which was attributed to the fact that HNTs filled part of the pore structure of the aerogel. Meanwhile, the role of skeleton of HNTs in the aerogels led to a steady enhancement of the compression modulus of the aerogel, which demonstrated the positive significance of HNTs in improving the compression modulus of the aerogel. Materials with a thermal conductivity of less than 50 mW/m·k were defined as efficient insulating materials.[46] As shown in Table 2, the thermal conductivity of PVA/CA/HNTs-0 was 0.057 W/m·k. This was due to the cross-linking of PVA with H_3BO_3 and the reaction of $CaCl_2$ with SA in the aerogel, which formed an interpenetrating network structure and thus gave it better thermal stability. With the addition of HNTs, the thermal conductivity of PVA aerogels decreased from 0.057W/m·k to 0.040W/m·k. The thermal conductivity of PVA/CA/HNTs-10 was significantly lower than that of PVA/CA/HNTs-0, which was because the HNTs had a nanometer-sized tubular pore structure inhibiting the solid-air-phase heat transfer and increasing the interfacial thermal resistance.

The stress−strain curves of the aerogels are shown in Figure 5. It could be seen that the elongation at break of PVA aerogel

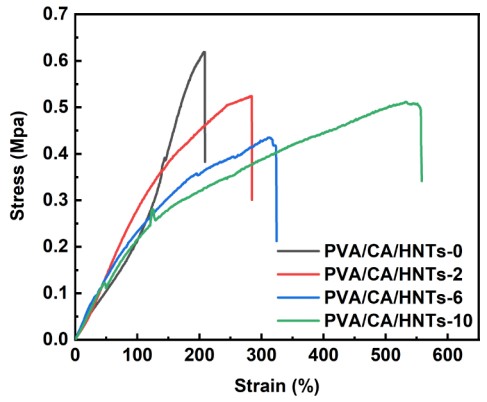

Figure 5. Stress−strain curves of the PVA aerogels.

increased and the tensile strength of aerogel decreased with the addition of HNTs. On the one hand, the active hydroxyl groups on the surface of HNTs had good compatibility with the hydroxyl groups on the molecular chain of PVA, which improved the tensile elongation of the PVA aerogels. On the other hand, the HNTs acted as a physical cross-linking point inside the PVA aerogels, which became a stress concentration point. When subjected to external force, the tensile strength was reduced.

3.4. Thermogravimetric Analysis of the PVA/CA/HNTs Aerogels. Figure 6 shows the thermogravimetric (TG) and differential thermogravimetric (DTG) curves of the PVA aerogels with detailed data referred to in Table S1. As shown in Figure 6a, the initial degradation temperature ($T_{5\%}$) of the PVA/CA/HNTs increased from 121.3 to 138.4 °C. The weight loss of PVA aerogel mainly occurred at 200−500 °C, and the residual char at 700 °C increased from 19.8% to 58.2% with the increase of HNTs content. Figure 6b shows that the thermal decomposition of PVA aerogel was mainly divided into two stages: The first thermal decomposition stage occurred between 200 and 300 °C, which was mainly the thermal decomposition of PVA; the second thermal decomposition stage occurred between 400 and 500 °C,[47,48] which was the whole thermal decomposition of PVA aerogel. Overall, the hollow tubular structure of halloysite nanotubes significantly improved the thermal stability of PVA/CA aerogels and endowed them with higher char residue and thermal decomposition temperatures.

3.5. Flame Retardancy of the PVA/CA/HNTs Aerogels. The flame-retardant properties of different PVA aerogels are shown in Tables 3 and 4. The t_1 and t_2, respectively, represented the combustion time after the first complete ignition and the combustion time again after first self-extinguishing. The UL-94 rating of the aerogel was maintained at V-0. This was mainly due to the presence of a large number of CA particles in the pore walls of the aerogel, which produced carbon dioxide through decarboxylation and created a dense carbon layer that prevented further combustion within the aerogel. It was worth noting that PVA/CA/HNTs-10 had a horizontal burning speed of less than 40 mm/min and an LOI of 60%. This was because HNTs had a hollow nanotube structure, which guaranteed the structural integrity of the carbon layer. And its low thermal conductivity could effectively reduce the efficiency of heat transfer. And so, combination of HNTs and CA improved the flame retardancy for PVA aerogels.

The cone calorimeter test (CCT) was an effective tool for evaluating flame-retardant materials and could be used to simulate real fire conditions.[49] The test results are shown in Figures 7a−d, and some important data are listed in Table 5, including the time to ignition (TTI), peak heat release rate (pHRR), total heat release (THR), total smoke production (TSP), and CO production (COP). Relative to PVA/CA/HNTs-0, PVA/CA/HNTs-10 showed a reduction in PHRR values from 144.16 kW/m^2 to 36.57 kW/m^2, THR values from 13.00 MJ/m^2 to 4.66 MJ/m^2, and TSP from 0.65 m^2 to 0.29 m^2. Furthermore, its COP value was also consistently low. After the cone calorimeter test, the digital photographs and SEM of the char residues are shown in Figure 8. For the PVA aerogel without HNTs (Figure 8a), it could not effectively inhibit the release of gas and heat, because it failed to form a continuous char layer. Furthermore, it had a severe surface shrinkage collapse. In contrast, the char layer of PVA aerogels containing HNTs (Figures 8b−d) was relatively compact and dense. Accompanied by the increase in the content of HNTs, the char layer gradually showed a pore structure (Figures 8a"−d"). It could be used as a barrier layer that was sufficient to protect the melted polymer from contact with fire and air, leaving the rest of the polymer unburned. This was mainly due to the high specific surface area of HNTs, which could form a carbon-nanotube-like flame-retardant network structure in the polymer matrix, resulting in a stable and dense char layer. The continuous char layer covered the surface of the aerogel, making it difficult for flammable gases generated by thermal

https://doi.org/10.1021/acsomega.4c04296
ACS Omega 2024, 9, 40608−40617

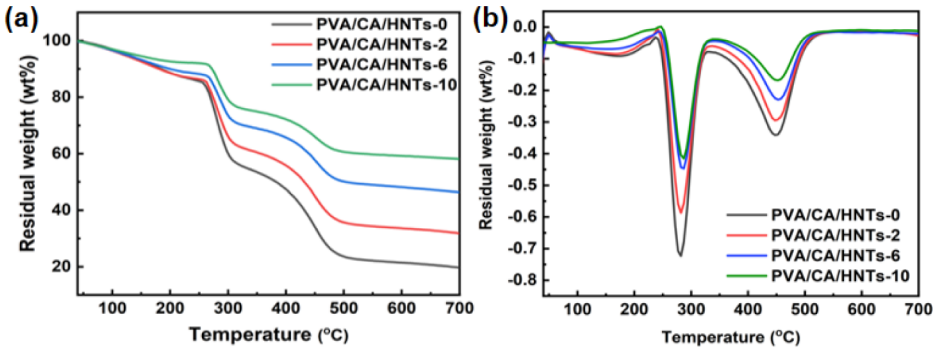

Figure 6. (a) Thermogravimetric (TG) and (b) differential thermogravimetric (DTG) curves of the PVA aerogels.

Table 3. Horizontal Combustion Test Results of Different PVA Aerogels

Sample	Burning duration (s)	Carbon layer length (mm)	Horizontal combustion rate ($mm \cdot s^{-1}$)
PVA/CA/HNTs-0	30	15	0.50
PVA/CA/HNTs-2		14	0.47
PVA/CA/HNTs-6		13	0.43
PVA/CA/HNTs-10		10	0.33

Table 4. UL-94 Test Results of Different the PVA Aerogels

Sample	t_1/t_2	Dripping	Ignite cotton	Rating	LOI (%)
PVA/CA/HNTs-0	5/1	No	No	V-0	43
PVA/CA/HNTs-2	3/1	No	No	V-0	52
PVA/CA/HNTs-6	3/0	No	No	V-0	54
PVA/CA/HNTs-10	1/0	No	No	V-0	60

Table 5. Cone Calorimeter Test Results of Different the PVA Aerogels

Sample	TTI (s)	pHRR (kW/m^2)	THR (MJ/m^2)	TSP (m^2)	TSR (m^2/m^2)
PVA/CA/HNTs-0	37	144.16	13.00	0.65	131.67
PVA/CA/HNTs-2	91	117.18	5.02	0.61	102.81
PVA/CA/HNTs-6	100	43.39	6.14	0.50	60.11
PVA/CA/HNTs-10	127	36.57	4.66	0.29	12.59

decomposition of the aerogel to escape and inhibiting the thermal decomposition of the aerogel. At the same time, the char layer with a pore structure also made it difficult for CO_2 from combustion to escape, gradually diluting the concentration of O_2 inside the aerogel. Meanwhile, according to the results of TG, it could also be proved that the more HNTs

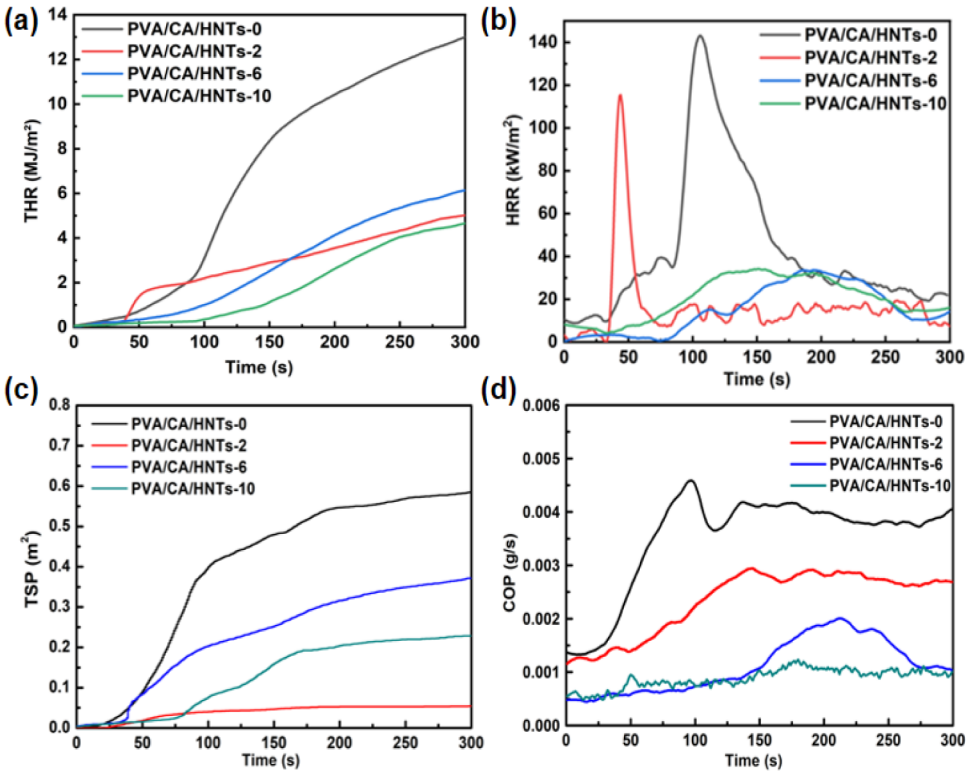

Figure 7. (a) HRR (b) THR (c) TSP (d) COP of the PVA aerogels.

https://doi.org/10.1021/acsomega.4c04296
ACS Omega 2024, 9, 40608−40617

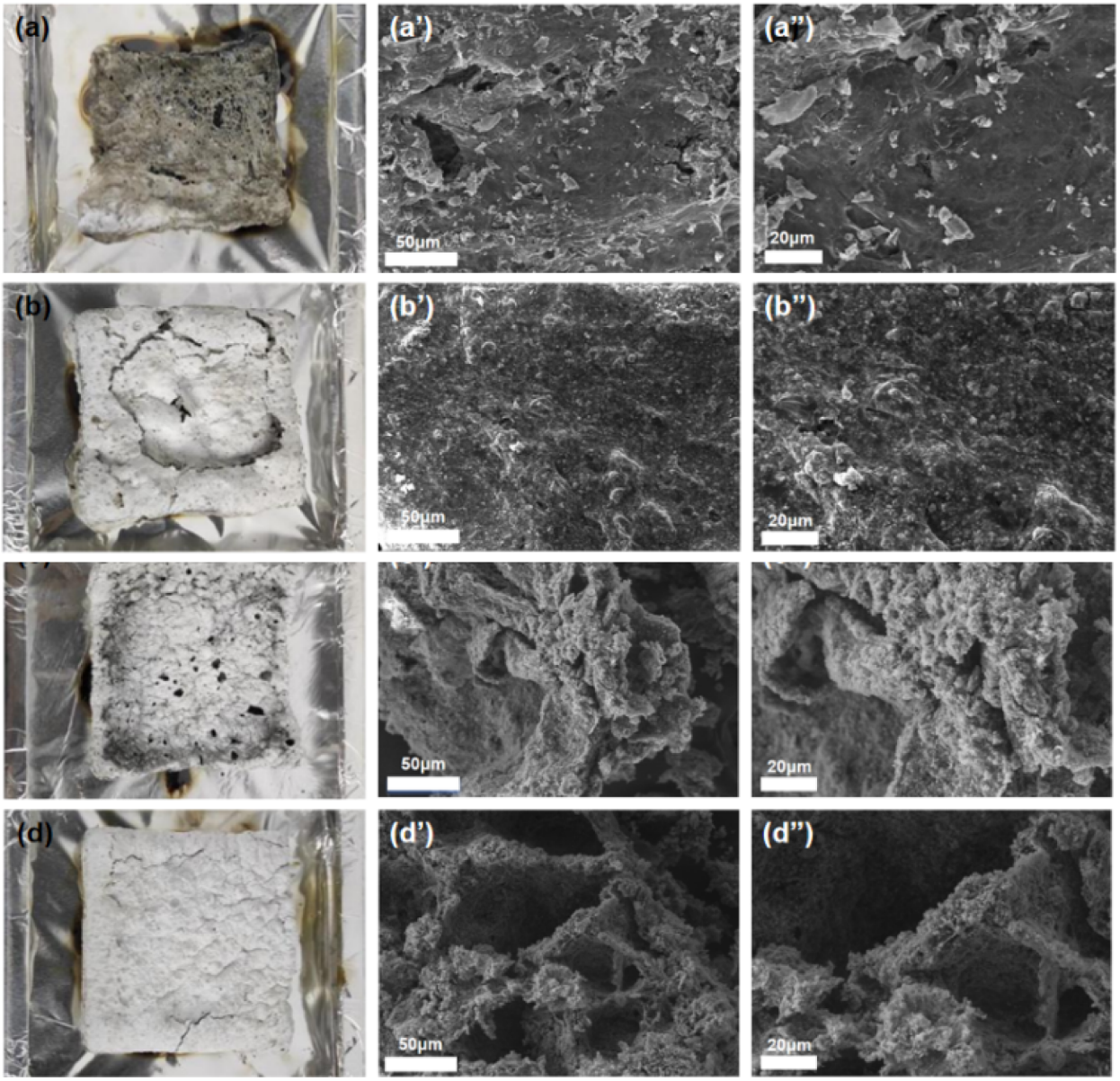

Figure 8. Digital photographs (a–d) and SEM (a'–d', a″–d") images of the residues for the PVA aerogels after cone calorimeter test. (a–a") PVA/CA/HNTs-0. (b–b") PVA/CA/HNTs-2. (c–c") PVA/CA/HNTs-6. (d–d") PVA/CA/HNTs-10.

were contained in the PVA aerogel, the higher the combustion residual carbon would be and the better the flame retardancy of the material would be.

In order to further investigate the flame-retardant and thermal insulation properties of PVA aerogels, 5 mm thick samples were prepared, and flame combustion experiments were carried out using a butane flame. Figure 9a shows the schematic diagram of the combustion experiment, and Figure 9b shows the maximum temperature of the backside of the aerogel as a function of time. The surface was exposed to a flame (800–1000 °C) for 25 min, and the temperature of the backside was measured every 5 min. The temperature of the back surface of PVA/CA/HTNs-10 and PVA/CA/HNTs-6 was 41.1 and 48.5 °C, respectively, which demonstrated that the aerogels not only had flame-retardant properties but also had excellent thermal insulation properties. The micron pores formed by the interpenetrating cross-linking network and the unique nanopores of HNTs together built up a multilevel pore structure inside the aerogel, efficiently inhibiting the exchange of substances and heat between the substrate and the outside world. Because of this, the thermal conductivity of the aerogel could be effectively reduced, and the thermal insulation performance was significantly improved. HNTs also played the role of skeleton support inside the aerogel, which synergized with PVA/CA to promote the formation of hybrid char barrier, effectively enhancing the flame-retardant performance. In addition, we compared the flame-retardant and thermal insulation performance parameters of PVA/CA/HNTs-10 in this work with recent reporting. As shown in Figure 9c,d and Table S2, lower values of THR, pHRR, and thermal conductivity and higher values of LOI represented better flame-retardant insulation properties of the samples. In this work, the flame-retardant and thermal insulation properties of PVA/CA aerogels were effectively enhanced by the addition of HNTs. The performances were not worse than other reported work.

https://doi.org/10.1021/acsomega.4c04296
ACS Omega 2024, 9, 40608–40617

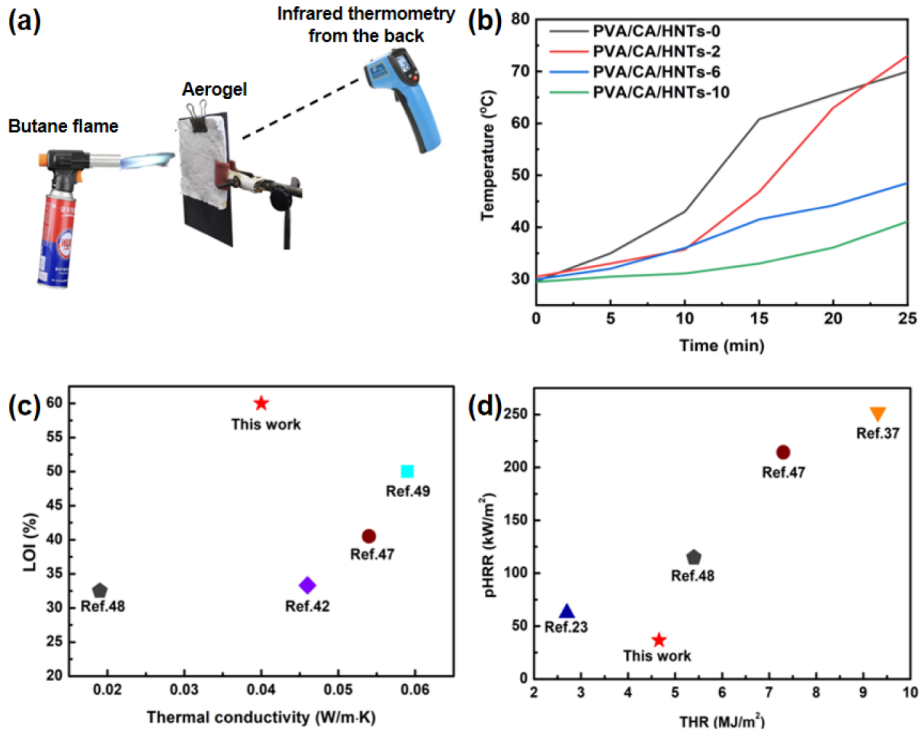

Figure 9. Fire resistance of the PVA aerogels. (a) Schematic of the fire resistance test. (b) Maximum temperature at the back of the aerogels versus time. (c, d) Schematic summary of flame-retardant and thermal insulation properties for aerogels reported in recent years.

4. CONCLUSION

The PVA aerogels with a hierarchical pore structure at the micrometer−nanometer scale were prepared by freeze-drying, in which HNTs were used as a reinforcing agent. The experimental results showed that the PVA/CA/HNTs aerogels exhibited excellent flame-retardant and thermal insulation properties and effectively reduced the heat release rate (HRR) and total heat release (THR) compared to the PVA/CA aerogels. In addition, PVA/CA/HNTs aerogels demonstrated a high LOI (60%) and a low thermal conductivity (0.040 W/m·k). Even when exposed to a flame (800−1000 °C) for 25 min, the temperature of the back surface remained below 80 °C. Incorporating HNTs with CA enhanced the flame retardancy of PVA by facilitating the formation of a dense carbon layer in the aerogel. In addition, the hierarchical pore structure inside the aerogel inhibited the exchange of substances and heat between the substrate and the outside world. As a flame-retardant and heat insulating material, PVA/CA/HNTs aerogel had promising development prospects and potential in the fields of construction, transportation, electronics, and electrical appliances.

■ ASSOCIATED CONTENT

Supporting Information

The Supporting Information is available free of charge at https://pubs.acs.org/doi/10.1021/acsomega.4c04296.

Relevant data of different PVA aerogels during TGA (Table S1), summary of flame-retardant and thermal insulation properties for aerogels reported in recent years (Table S2), and the macropore size distribution of the PVA aerogels with different addition of HNTs (Figure S1) (PDF)

■ AUTHOR INFORMATION

Corresponding Author

Jiayou Xu − *Department of Chemistry & Chemical Engineering, Guangzhou University, Guangzhou 510006, China*; orcid.org/0000-0002-4081-6261; Email: xujiayou516@163.com

Authors

Taopeng Yang − *Department of Chemistry & Chemical Engineering, Guangzhou University, Guangzhou 510006, China*

Shu Lv − *Department of Chemistry & Chemical Engineering, Guangzhou University, Guangzhou 510006, China*

Complete contact information is available at: https://pubs.acs.org/10.1021/acsomega.4c04296

Author Contributions

The manuscript was written through contributions of all authors. All authors have given approval to the final version of the manuscript.

Notes

The authors declare no competing financial interest.

■ ACKNOWLEDGMENTS

The authors appreciated the financial supports from Guangdong winner High-Tec & Industry Co., Ltd. and the Municipal Bureau of Science and Technology of Foshan, Guangdong Province, China [No.2016AG101374].

■ REFERENCES

(1) Yuan, C.; Wang, D.; Zhang, Y.; Li, K.; Ding, J. Research Progress on Preparation, Modification, and Application of Phenolic Aerogel. *Nanotechnol. Rev.* **2023**, *12* (1), 20230109.

https://doi.org/10.1021/acsomega.4c04296
ACS Omega 2024, 9, 40608−40617

(2) Karamikamkar, S.; Yalcintas, E. P.; Haghniaz, R.; De Barros, N. R.; Mecwan, M.; Nasiri, R.; Davoodi, E.; Nasrollahi, F.; Erdem, A.; Kang, H.; Lee, J.; Zhu, Y.; Ahadian, S.; Jucaud, V.; Maleki, H.; Dokmeci, M. R.; Kim, H.; Khademhosseini, A. Aerogel-Based Biomaterials for Biomedical Applications: From Fabrication Methods to Disease-Targeting Applications. *Adv. Sci.* **2023**, *10* (23), 2204681.
(3) Xiong, C.; Zhang, Y.; Ni, Y. Recent Progress on Development of Electrolyte and Aerogel Electrodes Applied in Supercapacitors. *J. Power Sources* **2023**, *560*, 232698.
(4) Ahmad, S.; Ahmad, S.; Sheikh, J. N. Silica Centered Aerogels as Advanced Functional Material and Their Applications: A Review. *J. Non-Cryst. Solids* **2023**, *611*, 122322.
(5) Sheng, Z.; Liu, Z.; Hou, Y.; Jiang, H.; Li, Y.; Li, G.; Zhang, X. The Rising Aerogel Fibers: Status, Challenges, and Opportunities. *Adv. Sci.* **2023**, *10* (9), 2205762.
(6) Wang, J.-X.; Xu, H.; Feng, J.-F.; Fan, S.-T.; Tan, M.; Ma, L.; Li, B.-J.; Zhang, S. Hydrophobic, elastic Cyclodextrin-Based Aerogel with Stable Broadband Sound Absorption. *Chem. Eng. J.* **2024**, *481*, 148480.
(7) Yang, L.; Chua, J. W.; Li, X.; Zhao, Y.; Thai, B. Q.; Yu, X.; Yang, Y.; Zhai, W. Superior Broadband Sound Absorption in Hierarchical Ultralight Graphene Oxide Aerogels Achieved through Emulsion Freeze-Casting. *Chem. Eng. J.* **2023**, *469*, 143896.
(8) Qu, W.; Wang, Z.; Qin, M.; Yang, X.; Zhang, F.; Wang, Z.; Ji, D.; Yu, D. Synthesis and Characterization of UiO-66-NH2 Incorporated PVA/Cellulose Nanofibers Composite Aerogel for Enhanced Oil−Water Separation and Formaldehyde Adsorption. *Sep. Purif. Technol.* **2023**, *325*, 124673.
(9) Zhang, W.; Liu, Y.; Tao, F.; An, Y.; Zhong, Y.; Liu, Z.; Hu, Z.; Zhang, X.; Wang, X. An Overview of Biomass-Based Oil/Water Separation Materials. *Sep. Purif. Technol.* **2023**, *316*, 123767.
(10) Chai, H.; Luo, J.; Li, J.; Zhong, Y.; Zhang, L.; Feng, X.; Xu, H.; Mao, Z. Lightweight and Robust Cellulose/MXene/Polyurethane Composite Aerogels as Personal Protective Wearable Devices for Electromagnetic Interference Shielding. *Int. J. Biol. Macromol.* **2024**, *271*, 132435.
(11) Wang, Y.-Y.; Zhang, F.; Li, N.; Shi, J.-F.; Jia, L.-C.; Yan, D.-X.; Li, Z.-M. Carbon-Based Aerogels and Foams for Electromagnetic Interference Shielding: A Review. *Carbon* **2023**, *205*, 10−26.
(12) Zhang, H.; Ma, H.; Ma, Y.; Lou, Y.; Jiao, Y.; Xu, J. Hierarchical Boric Acid/Melamine Aerogel Based on Reversible Hydrogen Bonds with Robust Fire Resistance, Thermal Insulation and Recycling Properties. *Composites, Part B* **2023**, *252*, 110507.
(13) Tao, J.; Yang, F.; Wu, T.; Shi, J.; Zhao, H.-B.; Rao, W. Thermal Insulation, Flame Retardancy, Smoke Suppression, and Reinforcement of Rigid Polyurethane Foam Enabled by Incorporating a P/Cu-Hybrid Silica Aerogel. *Chem. Eng. J.* **2023**, *461*, 142061.
(14) Sun, J.; Zhang, J.; Peng, X.; Zhang, X.; Yuan, Z.; Liu, X.; Liu, S.; Zhao, X.; Yu, S.; Yi, X. Carboxymethyl Cellulose/Polyvinyl Alcohol Composite Aerogel Supported Beta Molecular Sieve for CH4 Adsorption and Storage. *Carbohydr. Polym.* **2023**, *321*, 121246.
(15) Horvat, G.; Žvab, K.; Knez, Ž.; Novak, Z. Hybrid Polylactic-Acid−Pectin Aerogels: Synthesis, Structural Properties, and Drug Release. *Polymers* **2023**, *15* (2), 407.
(16) Hsan, N.; Kumar, S.; Koh, J.; Dutta, P. K. Chitosan Modified Multi-Walled Carbon Nanotubes and Arginine Aerogel for Enhanced Carbon Capture. *Int. J. Biol. Macromol.* **2023**, *252*, 126523.
(17) Huo, D.; Zhang, X.; Wei, J.; Wang, J.; Zhang, Q.; Yang, Q.; Zhu, H.; Zhang, F.; Fang, G.; Wu, T. Preparation and Characterization of Cellulose Nanofibril/Chitosan Aerogels with High-Adsorbability and Sensitive Indication for Indoor Free Formaldehyde. *Int. J. Biol. Macromol.* **2024**, *259*, 128891.
(18) Liu, C.; Liu, C.; Shi, Z.; Yu, D.; Wang, X.; Liu, S.; Wang, X.; Huang, F. A Peptide-Engineered Alginate Aerogel with Synergistic Blood-Absorbing and Platelet-Binding Capabilities to Rapidly Stop Bleeding. *Carbohydr. Polym.* **2023**, *321*, 121254.
(19) Sun, J.; Guo, J.; Li, Y.; Guan, F.; Zhang, Y.; Li, Z. Guar-Based Aerogels with Oriented Lamellar Structure and Lightweight Properties for Flame-Retardant and Thermal Insulation. *Int. J. Biol. Macromol.* **2024**, *256*, 128318.
(20) He, S.; Du, C.; Sheng, H.; He, C.; Liu, X.; Jin, X.; Chen, Q.; Tian, F. Ultrasensitive and Self-Powered Multiparameter Pressure−Temperature−Humidity Sensor Based on Ultra-Flexible Conductive Silica Aerogel. *Gels* **2023**, *9* (2), 162.
(21) Yang, M.; Lixia, Y.; Chen, Z.; Qiong, W.; Wang, Y.; Liu, T.; Li, M. Flexible Electrospun Strawberry-like Structure SiO2 Aerogel Nanofibers for Thermal Insulation. *Ceram. Int.* **2023**, *49* (6), 9165−9172.
(22) Rong, R.; Li, H.; Dong, X.; Hu, L.; Shi, X.; Du, Y.; Deng, H.; Sa, Y. Silk Fibroin-Chitosan Aerogel Reinforced by Nanofibers for Enhanced Osteogenic Differentiation in MC3T3-E1 Cells. *Int. J. Biol. Macromol.* **2023**, *233*, 123501.
(23) Wu, N.; Deng, S.; Wang, F.; Wang, M.; Xia, M.; Cui, H.; Jia, H. Highly Efficient Flame-Retardant and Enhanced PVA-Based Composite Aerogels through Interpenetrating Cross-Linking Networks. *Polymers* **2023**, *15* (3), 657.
(24) Zhao, Q.; Cheng, X.; Kang, J.; Kong, L.; Zhao, X.; He, X.; Li, J. Polyvinyl Alcohol Flame Retardant Film Based on Halloysite Nanotubes, Chitosan and Phytic Acid with Strong Mechanical and Anti-Ultraviolet Properties. *Int. J. Biol. Macromol.* **2023**, *246*, 125682.
(25) Ning, Y.; Liu, R.; Chi, W.; An, X.; Zhu, Q.; Xu, S.; Wang, L. A Chitosan Derivative/Phytic Acid Polyelectrolyte Complex Endowing Polyvinyl Alcohol Film with High Barrier, Flame-Retardant, and Antibacterial Effects. *Int. J. Biol. Macromol.* **2024**, *259*, 129240.
(26) Xiao, M.; Tan, M.; Peng, C.; Jiang, F.; Wu, K.; Liu, N.; Li, D.; Yao, X. Soft and Flexible Polyvinyl Alcohol/Pullulan Aerogels with Fast and High Water Absorption Capacity for Facial Mask Substrates. *Int. J. Biol. Macromol.* **2024**, *264*, 130469.
(27) Xu, W.; Xu, C.; Liu, J.; Ding, D.; Zhang, Y.; Zhou, Y. A Guanidine Phosphate-Assisted Boron Nitride Network Enabled Simultaneous Improvements in Flame Resistance and Thermal Conductivity of Polyvinyl Alcohol (PVA). *Polym. Degrad. Stab.* **2022**, *206*, 110178.
(28) Li, Y.-M.; Hu, W.-J.; Hu, S.-L.; Li, Y.-R.; Wang, D.-Y. Fabrication of Organic P-N Aerogel towards Simultaneously Super Thermal Insulation, Enhanced Compressive Strength, Flame Retardancy and Smoke Suppression for the Rigid Polyurethane Foam. *Chem. Eng. J.* **2023**, *474*, 145803.
(29) Yu, S.; Lu, S.; Tan, D.; Zhu, Y. Nitrogen and Phosphorus Co-Doped Carbon Dots for Developing Highly Flame Retardant Poly (Vinyl Alcohol) Composite Films. *Eur. Polym. J.* **2022**, *164*, 110970.
(30) Tang, D.; Zhu, L.; Li, X.; Liu, Y.; Wang, Q. Improved Flame Resistance and Thermal Insulation Properties of Steel Fireproof Coatings Based on Polyvinyl Alcohol @ Expandable Graphite. *Prog. Org. Coat* **2024**, *191*, 108444.
(31) Hu, J.; Xu, S.; Wang, Y.; Lai, X.; Xia, Z.; Zhang, Z.; Xie, P.; Zhang, S. Integration of Safety and Energy Storage: Experimental Study on Thermal and Flame-Retardant Properties of Ammonium Polyphosphate/Polyvinyl Alcohol/Modified Melamine Foam as a Composite Phase Change Material. *J. Energy Storage* **2024**, *84*, 110852.
(32) Tan, W.; Gao, L.; Su, J.; Zuo, C.; Ren, Y.; Liu, X. Phosphonitrile-Modified Biomass Multi-Crosslinking Strategy: Construction of Flame Retardant, Smoke Suppressive and Antibacterial Polyvinyl Alcohol Composites. *Composites, Part A* **2024**, *177*, 107897.
(33) Su, C.; Li, D.; Wang, L.; Wang, Y. Green Double Crosslinked Starch-Alginate Hydrogel Regulated by Sustained Calcium Ion-Gluconolactone Release for Human Motion Monitoring. *Chem. Eng. J.* **2023**, *455*, 140653.
(34) He, L.; Bao, G.; Yu, X.; Zhang, X.; Jin, X.; Yu, Z.; He, Y.; Zhang, R.; Qin, D. A Green and Eco-Friendly Method to Enhance Bamboo Flame Resistance via Calcium Alginate Assisted in-Situ Mineralization of Hydroxyapatite. *Chem. Eng. J.* **2024**, *485*, 149765.
(35) Xu, Y.-J.; Qu, L.-Y.; Liu, Y.; Zhu, P. An Overview of Alginates as Flame-Retardant Materials: Pyrolysis Behaviors, Flame Retardancy, and Applications. *Carbohydr. Polym.* **2021**, *260*, 117827.

https://doi.org/10.1021/acsomega.4c04296
ACS Omega 2024, 9, 40608−40617

(36) Tian, R.; Gao, S.; Li, K.; Lu, C. Design of Mechanical-Robust Phosphorescence Materials through Covalent Click Reaction. *Nat. Commun.* **2023**, *14* (1), 4720.
(37) Cao, X.; Chen, D.; Tiwari, S. K.; Wei, F.; Chen, Y.; Thummavichai, K.; Wang, N.; Yan, C.; Zhu, Y. Implanting MOF Co-Doped Carbon Nanotubes into PVP as Flame-Retardant to Fabricate High Performance PVA/SA Aerogel Nanocomposites. *J. Environ. Chem. Eng.* **2024**, *12* (2), 111977.
(38) Zhang, Z.; Zhou, Z.; Huang, J.; Wang, Y. A Flame Retardant Poly Vinyl Alcohol/Graphene Oxide/Phytic Acid Composite for a Quick Response and Ultra-Long Fire Alarm. *J. Mater. Chem. A* **2024**, *12*, 6050.
(39) Lv, Q.; Yang, J.; Sun, X.; Tang, H.; Wang, L. Preparation of Highly Efficient Thermal Insulating Halloysite Nanotubes/Polyvinyl Alcohol Composite Aerogel Based on a Simple Freeze-drying Strategy. *Polym. Compos.* **2023**, *44* (3), 1648−1657.
(40) Zou, D.; Zhou, Y.; Yan, W.; Zhou, Y.; Gao, C. Boric Acid-Loosened Polyvinyl Alcohol/Glutaraldehyde Membrane with High Flux and Selectivity for Monovalent/Divalent Salt Separation. *J. Membr. Sci.* **2022**, *662*, 120954.
(41) Wang, C.; Zhang, Z.; Ma, Z.; Zhou, Z.; Huang, J.; Wang, Y. Flame-resistant and Tough Polyvinyl Alcohol Film with Ultraviolet-absorbing Capacity. *J. Appl. Polym. Sci.* **2023**, *140* (31), No. e54215.
(42) Yang, Z.; Zhu, D. Synthesis and Characterization of AlCl3-Chitosan Composite Aerogels Incorporating Polyvinyl Alcohol and Bentonite Clay. *J. Sol-Gel Sci. Technol.* **2022**, *103* (3), 722−729.
(43) Hong, J.; Hong, Y.; Jeong, J.; Oh, D.; Goh, M. Robust Biobased Vitrimers and Its Application to Closed-Loop Recyclable Carbon Fiber-Reinforced Composites. *ACS Sustainable Chem. Eng.* **2023**, *11* (38), 14112−14123.
(44) Liu, J.; Shang, S.; Jiang, Z.; Zhang, R.; Sui, S.; Zhu, P. Facile Fabrication of Chemically Modified Sodium Alginate Fibers With Enhanced Mechanical Performance. *AATCC J. Res.* **2022**, *9* (1), 35−42.
(45) Luo, M.; Lin, J.; Zhou, X.; Pu, X. Study on Physical Properties of Four pH Responsive Spodoptera Exigua Multiple Nucleopolyhedrovirus (SeMNPV) Microcapsules as Controlled Release Carriers. *Sci. Rep.* **2022**, *12* (1), 21873.
(46) Liu, M.; Cheng, G.; Tang, Z.; Zhou, L.; Wan, X.; Ding, G. Flame retardancy performance and mechanism of polyvinyl alcohol films grafted amino acid ionic liquids with high transparency and excellent flexibility. *Polym. Degrad. Stab.* **2022**, *205*, 110133.
(47) Zhang, C.; Hu, Y.; Shao, J.; Pan, H. Flame Retardant Cellulose/Polyvinyl Alcohol/Sodium Alginate Composite Aerogels Crosslinked by Metal Ions for Flame Resistance Materials. *Cellulose* **2023**, *30* (11), 7079−7093.
(48) Li, M.; Zhu, Z.; Jiao, R.; Chen, Y.; Cao, X.; Sun, H.; Li, J.; Li, A. Preparation of DOPO-KH550 Modified Hollow Glass Microspheres/PVA Composite Aerogel for Thermal Insulation and Flame Retardancy. *J. Colloid Interface Sci.* **2024**, *654*, 719−730.
(49) Liao, W.; Li, Z.; Yang, L. Cross Network Composite Aerogel Towards Robust and Fire-Resist Thermal Insulation Material. *Adv. Eng. Mater.* **2023**, *25* (9), 2201443.

https://doi.org/10.1021/acsomega.4c04296
ACS Omega 2024, 9, 40608−40617